Hindawi Publishing Corporation
Journal of Nanomaterials
Volume 2015, Article ID 326294, 9 pages
http://dx.doi.org/10.1155/2015/326294

Research Article

Tuning Electronic Structures of BN and C Double-Wall Hetero-Nanotubes

Xueran Liu, Meijun Han, Xinjiang Zhang, Haijun Hou, Shaoping Pang, and Qisheng Wu

School of Materials Engineering, Yancheng Institute of Technology, Yancheng, Jiangsu 224051, China

Correspondence should be addressed to Shaoping Pang; psp800@126.com and Qisheng Wu; qishengwu@ycit.cn

Received 8 April 2015; Revised 15 June 2015; Accepted 2 July 2015

Academic Editor: Dan Xia

First principle calculations based on density functional theory with the generalized gradient approximation were carried out to investigate the energetic and electronic properties of carbon and boron nitride double-wall hetero-nanotubes (C/BN-DWHNTs) with different chirality and size, including an armchair (n, n) carbon nanotube (CNT) enclosed in (m, m) boron nitride nanotube (BNNT) and a zigzag (n, 0) CNT enclosed in (m, 0) BNNT. The electronic structure of these DWHNTs under a transverse electric field was also investigated. The ability to tune the band gap with changing the intertube distance (d_i) and imposing an external electric field (F) of zigzag DWHNTs provides the possibility for future electronic and electrooptic nanodevice applications.

1. Introduction

Carbon nanotubes (CNTs) play a very important role in nanodevice applications due to their novel properties. by comparison with CNTs, boron nitride nanotubes (BNNTs) are formed with similar structures, however, of very distinctive properties [1]. Of similar crystalline structure, hexagonal boron nitride (h-BN) has been considered as a potential substrate material for graphene [1, 2]. Recently, the structures of bilayer and trilayer graphene/h-BN have been reported with tunable band gaps for electronic device applications [3–5].

Hexagonal boron nitride shares similar crystalline structure with graphene, and it is slightly lattice-mismatched from graphene by about 1.5%, which implies that it is possible to form hetero-nanostructures. BNNTs' growth on CNT has successfully been applied to nanowires [6]. Several studies have also been conducted on BN-coated CNTs [7, 8]. The BNNT around the CNTs effectively helps to protect them and makes them more stable; for example, oxidation degradation of CNTs is reduced by coating with BNNTs, and the thermal stability of CNT@BNNTs is far superior to CNTs [9].

An efficient way to modify the band gap of nanotubes is to apply an external electric field F [10]. The response of the nanotube to F is of interest for studying its future application, such as that in logic gates, static memory cells, and sensor devices [11–13]. Ab initio calculation showed that band gaps of both CNTs and BNNTs can be greatly reduced by a transverse electric filed [14, 15]. An intriguing question to answer is whether external electric fields can also be an efficient way to modulate the electronic properties of C/BN-DWHNTs.

However, a first-principles study on the stability as well as the electronic properties modulated with d_i and F of C/BN-DWHNTs is not available. To fill the deficiency, in this work, we performed a series of first-principles calculations to study the coaxial CNT@BNNT and to examine the electric field shielding effect of BNNT on the inside CNT. We calculated the band structures of coaxial CNT@BNNT consisting of armchair and zigzag CNT cores and BNNT sheaths, focusing on the band structure variations with d_i and F. The relative insensitivity of armchair CNT@BNNT to F, at least for the few cases considered here, suggests that zigzag CNT@BNNT would be a suitable candidate for double-wall hetero-nanotubes devices.

2. Calculation Methods

The geometric structure optimization and calculation of the related electrical properties of the CNT@BNNT with no F were conducted using SIESTA [16, 17] and adopted norm-conserving nonlocal pseudopotentials for the atomic core.

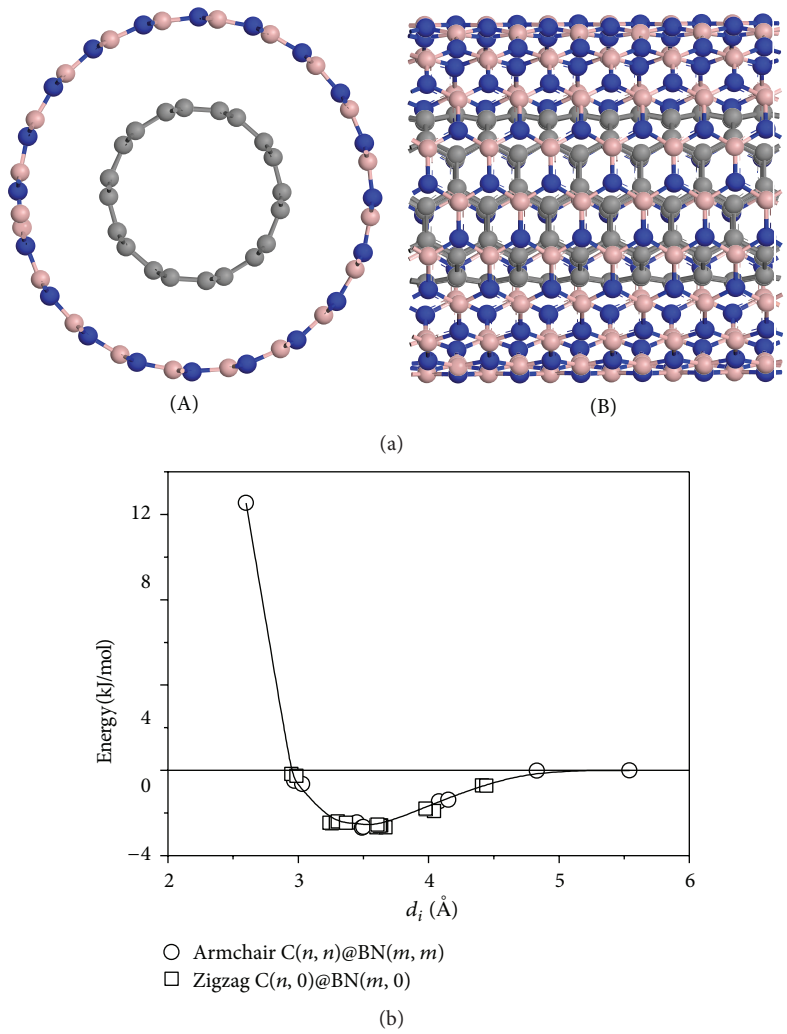

FIGURE 1: Structure of the optimized CNT(5, 5)@BNNT(10, 10): (a) top view (A) and side view (B). (b) The formation energy E_f variation versus intertube distance d_i. ○ and □ are the formation energy of calculated armchair and zigzag DWHNTs, respectively. The solid line was plotted in eyes.

The Perdew, Burke, and Ernzerhof (PBE) form generalized gradient approximation (GGA) corrections were employed for the exchange-correlation potential energy [18]. The atomic orbital basis set employed throughout was double-ζ plus polarization functions (DZP). Periodic boundary condition along the axis was employed for nanotubes. Brillouin zones were sampled by a set of k-points grid ($1 \times 1 \times 8$) according to the Monkhorst-Pack approximation [19].

When electric field was imposed, the calculation was using density functional theory available in DMol3 code [20, 21]. The PBE function [22] of GGA was used to calculate the exchange-correlation potential energy, the all electron approach was used, and the orbit population parameter smearing was set at 0.0005 a.u.

Our models were constructed within a tetragonal super cell with lattice constants of a and b equaling 40 Å to avoid the interaction between two adjacent nanotubes and c, the lattice constant in z direction along the tube axis, equaling one-dimensional (1D) lattice parameter of the nanotubes. The tube was taken along the z direction and the circular cross section was lying in the (x, y) plane. Both the CNT and BNNTs structures were fully optimized until the force on each atom was less than 0.005 eV $Å^{-1}$ during relaxation.

The van der Waals interactions are very important in two-dimensional materials [23], especially in layered structures. The van der Waals force has obvious effect on the adsorption energy and adsorption position and height [24–26]. In this paper, the distances of the CNT and BNNT are fixed, and the optimization does not change the C/BN-DWHNTs structures. The van der Waals interactions could increase the value of E_f, but they should not affect the electronic properties of C/BN-DWHNTs [10].

3. Results and Discussion

Two types of C/BN-DWHNTs were investigated, zigzag and armchair. The zigzag C/BN-DWHNTs are studies that include CNT(n, 0)@BNNT(m, 0) (n = 6–10, m = 14–20).

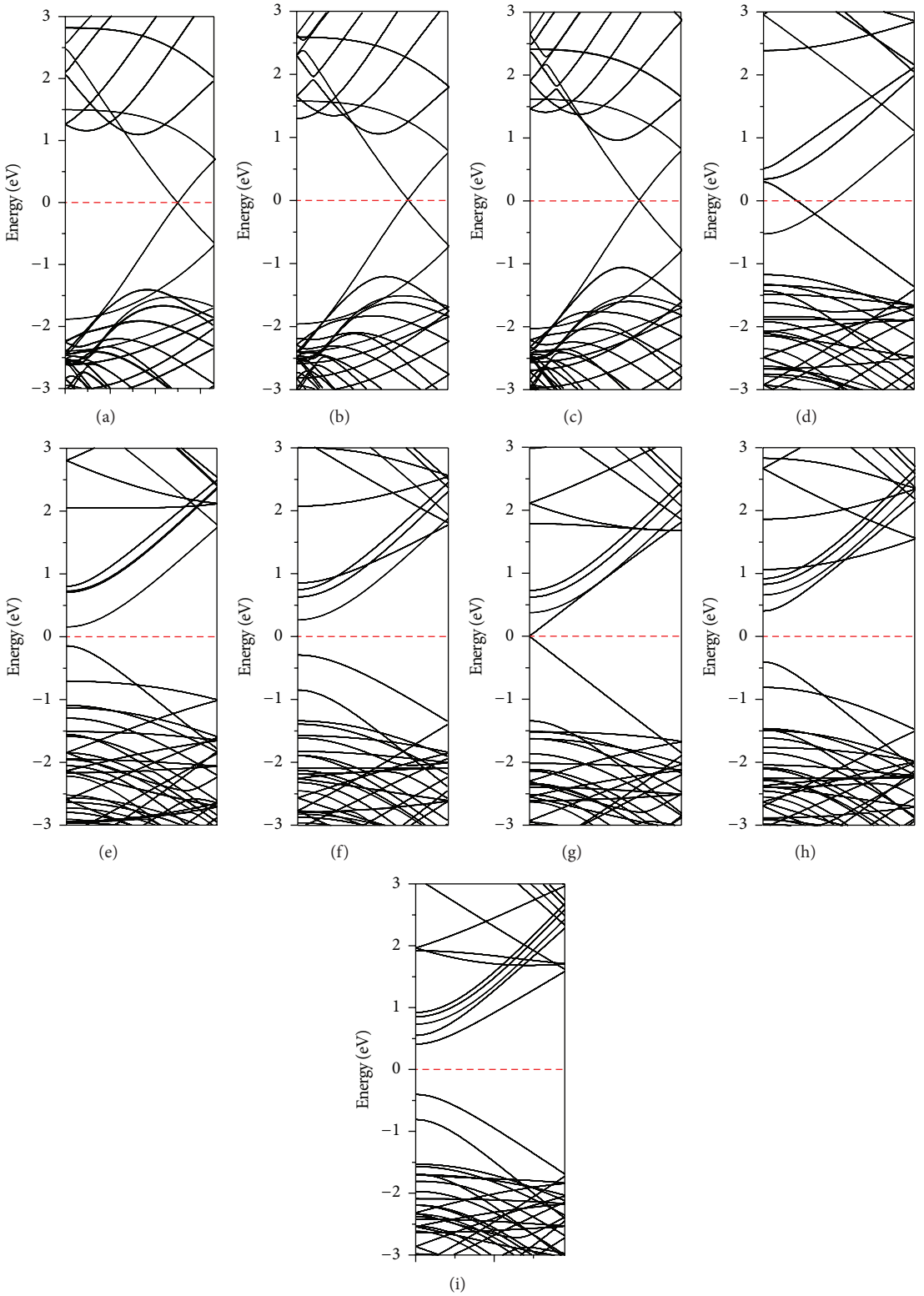

Figure 2: Band structures of (a) armchair CNT(5, 5)@BNNT(10, 10), (b) armchair CNT(6, 6)@BNNT(11, 11), (c) armchair CNT(7, 7)@BNNT(12, 12), (d) zigzag CNT(6, 0)@BNNT(15, 0), (e) zigzag CNT(7, 0)@BNNT(16, 0), (f) zigzag CNT(8, 0)@BNNT(17, 0), (g) zigzag CNT(9, 0)@BNNT(18, 0), (h) zigzag CNT(10, 0)@BNNT(19, 0), and (i) zigzag CNT(11, 0)@BNNT(20, 0).

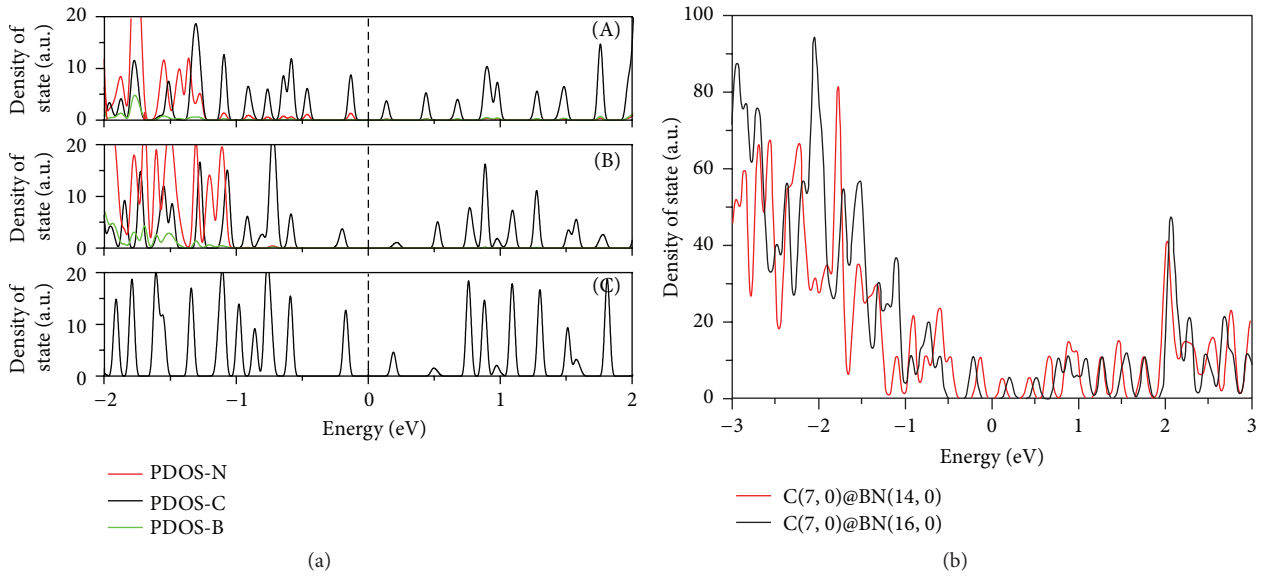

FIGURE 3: (a) (A) Partial density of state of zigzag CNT(7, 0)@BNNT(14, 0), (B) partial density of state of zigzag CNT(7, 0)@BNNT(16, 0), and (C) density of state of single-wall CNT (7, 0). The Fermi level lies at 0 eV (dash line). (b) Density of state of CNT(7, 0)@BNNT(14, 0) and CNT(7, 0)@BNNT(16, 0) DWHNTs.

The armchair C/BN-DWHNTs considered are CNT(n, n)@BNNT(m, m) (n = 5–7, m = 8–13). Figure 1(a) gives an illustration of the coaxial armchair CNT(5, 5) inside armchair BNNT(10, 10), the left (right) panel for the top (lateral) view of the initial structure.

The calculated covalent bond lengths of the various C/BN-DWHNTs in the fully optimized structures are listed in Table 1. For any C/BN-DWHNTs, we define the binding energy per atom as $E_b = [E_t^@ - xE^C - y(E^B + E^N)]/(x + y)$, where E^C, E^B, and E^N are the energy of isolated carbon, boron, and nitride atoms, respectively. $E_t^@$ is the total energy of a C/BN-DWHNT, x is the number of C atoms, and y is the number of B and N atoms. The formation energy E_f ($E_f = E_b^@ - E_b^C - E_b^{BN}$) of each C/BN-DWHNT is also calculated, in which the E_b^C and E_b^{BN} are the binding energy of free standing CNT and BNNT, respectively.

The stability of C/BN-DWHNTs is determined by the interaction force between the inner and outer nanotubes, as shown in Table 1. The formation energy E_f varying with d_i was plotted in Figure 1(b). When d_i = ~2.60 Å, E_f is positive, which means the free standing CNT and BNNT are favorite in energy. When d_i = ~3.5 Å, the armchair C/BN-DWHNTs have the lowest binding energy and formation energy, meaning that the armchair C/BN-DWHNTs at d_i = ~3.5 Å are more possible to exist. This result is in agreement with the literature [27], in which Yuan and Liew have studied the coaxial CNT@BNNT nanocables and found that the optimal intertube distances between inner C tube and the outer BN are about 3.5 Å for armchair nanocables.

The distance d_i of the armchair C/BN-DWHNTs can be approximately evaluated by the expression as $d_i = 3(ma_{B\text{-}N} - na_{C\text{-}C})/2\pi$; here $a_{B\text{-}N}$ and $a_{C\text{-}C}$ are the bond lengths of outer BNNT and inner CNT, respectively. Let d_i = 3.5 Å; the possible stable structures are CNT(n, n)@BNNT(m, m) ($m - n$ = 5), for example, CNT(5, 5)@BNNT(10, 10), CNT(6, 6)@BNNT(11, 11), and CNT(7, 7)@BNNT(12, 12) DWHNTs (see Table 1(a)). Taking the armchair CNT(5, 5)@BNNT(m, m) (m = 8–13) nanotubes as examples, the covalent bond lengths in the fully optimized CNT and BNNT are 1.43 and 1.45 Å, respectively. When d_i = ~2.60 Å, the bond length of inner CNT was suppressed to 1.385 Å and the bond length of outer BNNT was extended to 1.540 Å in the perpendicular direction. This result indicates the occurrence of greater repulsive interactions between the inner CNT and the outer BNNT.

The calculated covalent bond lengths of the various zigzag DWHNTs in fully optimized structures are listed in Table 1(b). When d_i = ~3.6 Å, the zigzag C/BN-DWHNTs have the lowest binding energy and formation energy. It means that the C/BN-DWHNTs at d_i = ~3.6 Å are more possible to exist. For zigzag configurations, the distance d_i is as follows: $d = \sqrt{3}\,(ma_{B\text{-}N} - na_{C\text{-}C})/2\pi$; letting d = 3.6 Å, the possible stable structures are CNT(n, 0)@BNNT(m, 0) ($m - n$ = 9), for example, CNT(6, 0)@BNNT(15, 0), CNT(7, 0)@BNNT(16, 0) DWHNTs.

The calculated band structures of C/BN-DWHNTs are shown in Figure 2. The armchair C/BN-DWHNTs are metallic, with the lowest conduction band and the highest valence band crossing over the Fermi level at ~2/3 along Γ-Z direction in reciprocal space. The electric band structure near the Femi level is very similar to the CNTs because the lowest conduction band and the highest valence band are determined by the carbon atoms. We also found that changing d_i cannot be an efficient way to open the band gap for armchair C/BN-DWHNTs.

The calculated band gaps (E_g) of the single-wall CNT(n, 0) are 0.19, 0.58, 0.04, 0.78, and 0.87 eV for n = 7–11,

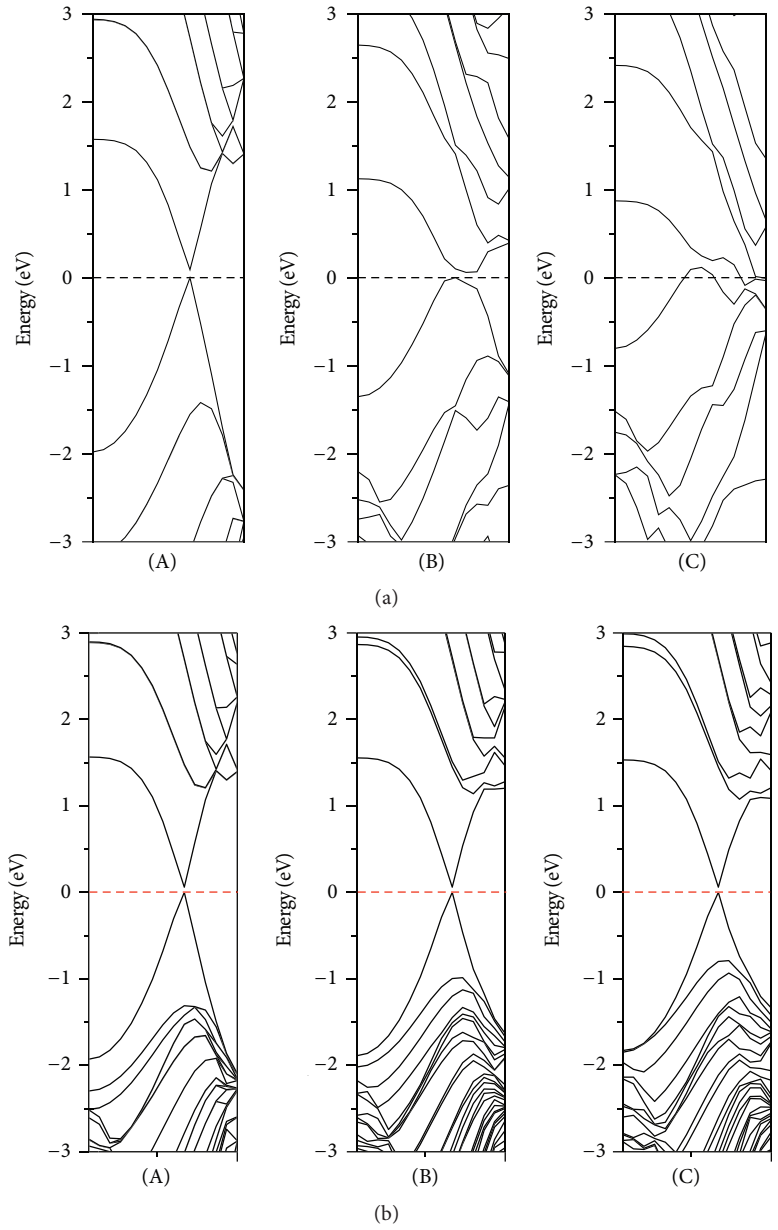

Figure 4: (a) Band structures of CNT(5, 5) under an external electric field of (A) $F = 0$ V/Å, (B) $F = 0.1$ V/Å, and (C) $F = 0.15$ V/Å along y-axis, respectively. (b) Band structures for CNT(5, 5)@BNNT(10, 10) under (A) $F = 0$ V/Å, (B) $F = 0.1$ V/Å, and (C) $F = 0.15$ V/Å along y-axis, respectively.

respectively, which are consistent with results of similar studies [28]. For the zigzag DWHNTs, d_i affects the band gap of C/BN-DWHNTs. A different size CNT(7, 0) was considered as the inner tube of the zigzag C/BN-DWHNTs. The calculated band gaps are listed in Table 1(b). All the zigzag CNT(7, 0)@BNNT structures are found to be direct gap semiconductors with both the valence band top and conduction band bottom at the Γ point. In Figure 3(a), analysis of the PDOS of CNT(7, 0)@BNNT indicated that p orbitals of the carbon atoms dominate the band near Femi level. However, for CNT(7, 0)@BNNT(14, 0), the p orbitals of the nitrogen atoms have a contribution to the bands near the Femi level, which also proved the stronger interaction when the d_i strayed from ~3.6 Å. Figure 3(b) shows the DOS of CNT(7, 0)@BNNT(14, 0) and CNT(7, 0)@BNNT(16, 0) DWHNTs. The band gap of CNT(7, 0)@BNNT(14, 0) became small when comparing with the CNT(7, 0)@BNNT(16, 0) during the stronger intertube interactions.

After the CNTs were encapsulated into the BNNT, for the stable structure such as CNT(5, 5)@BNNT(10, 10), their geometries changed little. To study the effect of the transverse electric field on the electronic structure of the nanotubes, F along y direction (perpendicular to the tube axis) was imposed. We first examined the electronic properties of

Table 1: (a) Calculated bond lengths ($a_{C\text{-}C}$ and $a_{B\text{-}N}$) in the direction of the tube axis (z) and in the perpendicular direction (r), intertube spacing (d_i), the unit being Å, the binding energy (E_b), and the forming energy (E_f) in kJ/mol of different geometrically optimized armchair double-wall hetero-nanotube optimizations. (b) Calculated bond lengths ($a_{C\text{-}C}$ and $a_{B\text{-}N}$) in the perpendicular direction (r), intertube spacing (d_i), the unit being Å, the binding energy (E_b kJ/mol) and the forming energy (E_f kJ/mol) kJmol^{-1}, and GGA band gap (E_g eV) of different geometrically optimized zigzag double-wall hetero-nanotube optimizations. (c) The calculated bond lengths ($a_{C\text{-}C}$ and $a_{B\text{-}N}$) of various double-wall hetero-nanotubes, in the direction of the tube axis (z) and in the perpendicular direction (r), and intertube spacing (d_i) of different geometrically optimized double-wall hetero-nanotube optimizations; the unit is Å.

(a)

	$a_{C\text{-}C}$		$a_{B\text{-}N}$		d_i	E_b	E_f
	r	z	r	z			
CNT(5, 5)@BNNT(8, 8)	1.385	1.418	1.540	1.471	2.60	−761.89	12.537
CNT(5, 5)@BNNT(9, 9)	1.420	1.434	1.473	1.453	2.97	−773.74	−0.493
CNT(5, 5)@BNNT(10, 10)	1.435	1.441	1.439	1.441	3.45	−774.41	−2.450
CNT(5, 5)@BNNT(11, 11)	1.441	1.443	1.438	1.441	4.08	−772.29	−1.455
CNT(5, 5)@BNNT(12, 12)	1.436	1.440	1.444	1.442	4.83	−769.60	−0.023
CNT(5, 5)@BNNT(13, 13)	1.434	1.440	1.448	1.444	5.54	−768.83	−0.013
CNT(6, 6)@BNNT(10, 10)	1.416	1.431	1.473	1.453	3.03	−777.50	−0.641
CNT(6, 6)@BNNT(11, 11)	1.433	1.440	1.446	1.445	3.49	−778.17	−2.689
CNT(6, 6)@BNNT(12, 12)	1.440	1.444	1.439	1.441	4.15	−775.66	−1.376
CNT(7, 7)@BNNT(12, 12)	1.431	1.438	1.448	1.445	3.50	−780.77	−2.657

(b)

	$a_{C\text{-}C}$	$a_{B\text{-}N}$	d_i	E_b	E_f	E_g
	r	r				
CNT(6, 0)@BNNT(13, 0)	1.439	1.466	2.947	−763.81	−0.173	Metallic
CNT(6, 0)@BNNT(14, 0)	1.450	1.452	3.260	−765.74	−2.488	Metallic
CNT(6, 0)@BNNT(15, 0)	1.450	1.447	3.601	−765.55	−2.678	Metallic
CNT(6, 0)@BNNT(16, 0)	1.458	1.445	4.043	−764.40	−1.919	Metallic
CNT(6, 0)@BNNT(17, 0)	1.458	1.443	4.412	−762.85	−0.705	Metallic
CNT(7, 0)@BNNT(14, 0)	1.431	1.466	2.987	−768.25	−0.271	0.146
CNT(7, 0)@BNNT(15, 0)	1.440	1.453	3.240	−769.60	−2.457	0.247
CNT(7, 0)@BNNT(16, 0)	1.446	1.446	3.670	−769.50	−2.685	0.302
CNT(7, 0)@BNNT(17, 0)	1.449	1.443	3.979	−768.25	−1.829	0.281
CNT(7, 0)@BNNT(18, 0)	1.449	1.442	4.444	−766.51	−0.731	0.262
CNT(8, 0)@BNNT(16, 0)	1.439	1.453	3.288	−773.45	−2.467	0.492
CNT(8, 0)@BNNT(17, 0)	1.444	1.446	3.636	−772.49	−2.581	0.558
CNT(9, 0)@BNNT(17, 0)	1.436	1.453	3.305	−775.66	−2.395	0.034
CNT(9, 0)@BNNT(18, 0)	1.443	1.445	3.627	−775.09	−2.608	0.027
CNT(10, 0)@BNNT(18, 0)	1.434	1.452	3.368	−777.78	−2.471	0.805
CNT(10, 0)@BNNT(19, 0)	1.441	1.444	3.603	−777.11	−2.571	0.811
CNT(11, 0)@BNNT(20, 0)	1.442	1.444	3.610	−776.15	−2.558	0.814
CNT(11, 0)@BNNT(21, 0)	1.441	1.442	3.976	−777.30	−1.799	0.808

(c)

CNT(5, 5)@BNNT(10, 10)			
E (V/Å)	0	0.1	0.25
$a_{C\text{-}C}{}^{z}$	1.435	1.433–1.437	1.439–1.431
$a_{C\text{-}C}{}^{r}$	1.435	1.434–1.436	1.433–1.440
$a_{B\text{-}N}{}^{z}$	1.439	1.434–1.440	1.429–1.447
$a_{B\text{-}N}{}^{r}$	1.441	1.447–1.472	1.438–1.508
d_{ix}	3.592	3.614	3.697
d_{iy}	3.602	3.597	3.581
CNT(5, 5)			
E (V/Å)	0	0.1	0.25 (distortion)
$a_{C\text{-}C}{}^{z}$	1.425	1.424–1.428	1.421–1.437
$a_{C\text{-}C}{}^{r}$	1.426	1.426–1.431	1.392–1.476
BNNT(10, 10)			
E (V/Å)	0	0.1	0.25
$a_{C\text{-}C}{}^{z}$	1.436	1.435–1.437	1.436–1.444
$a_{C\text{-}C}{}^{r}$	1.452	1.447–1.452	1.432–1.457

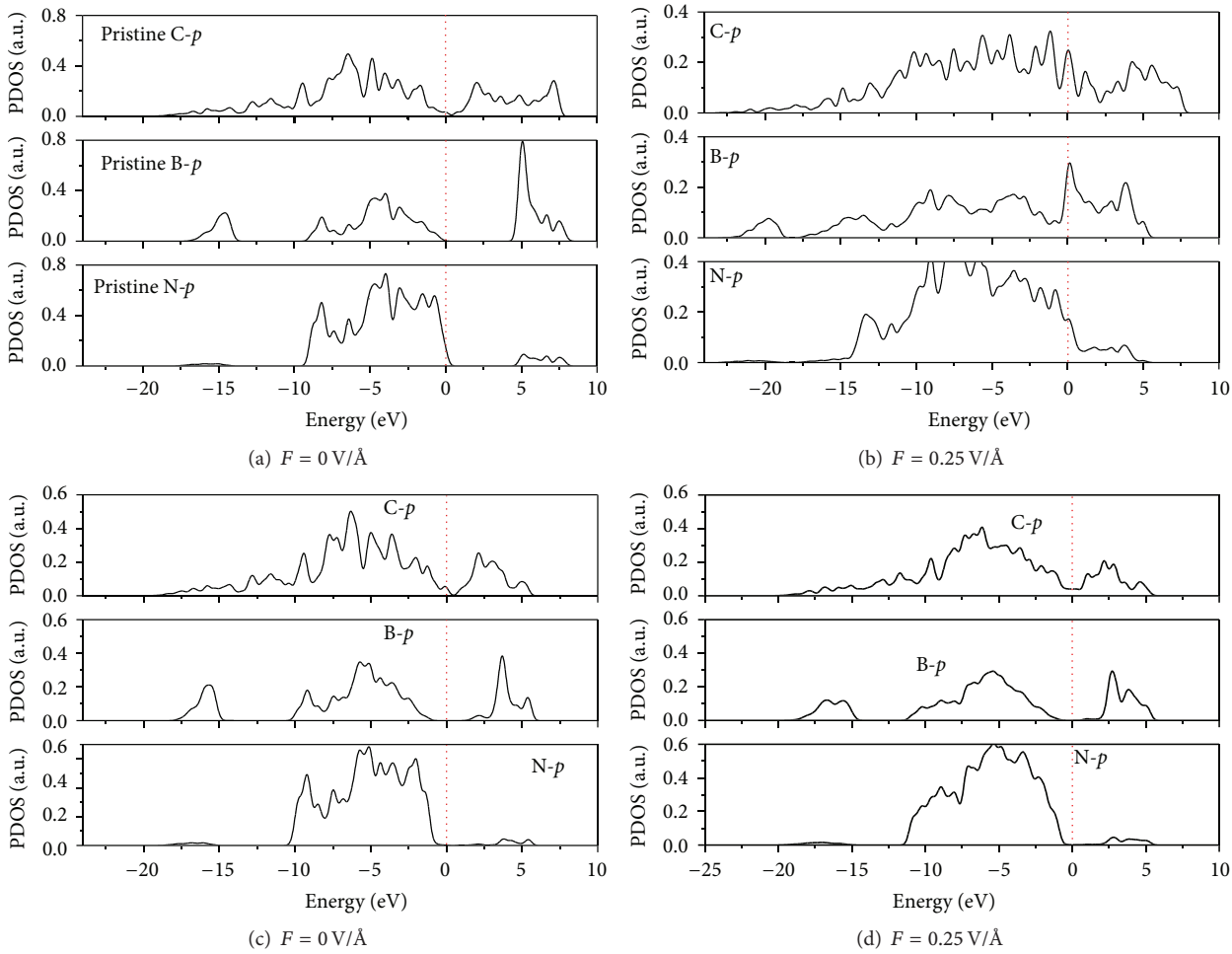

Figure 5: PDOS of CNT(5, 5) and BNNT(10, 10) under an external electric field of (a) $F = 0$ V/Å and (b) $F = 0.25$ V/Å, respectively. PDOS of CNT(5, 5)@BNNT(10, 10) under an external electric field of (c) $F = 0$ V/Å and (d) $F = 0.25$ V/Å, respectively. The Fermi level lies at 0 eV (dotted line). The solid line corresponds to p-state of C, B, and N at pristine CNT(5, 5) and BNNT(10, 10), respectively.

the CNT(5, 5) under an electronic field (see Figure 4(a)). The CNT(5, 5) remains semimetallic with an enhancement of density of states around the Fermi level with increasing the eternal electrical field. Two linear bands became flat (localized) around the Femi level in CNT(5, 5) with increasing field strengths. It can therefore be inferred that the conductance will be greatly enhanced. And the results were well consistent with the literature [29]. The calculated values of the band structures for the armchair CNT(5, 5)@BNNT(10, 10) at $F = 0$, 0.1 and 0.15 V/Å are presented in Figure 4(b). There is no distinct difference between the electronic structures of the CNT(5, 5)@BNNT(10, 10) under different transverse electric fields. It shows that the transverse field does not affect the electric structures evidently. Whereas the band structures for CNT(5, 5) under $F = 0$ and $F = 0.25$ V/Å show a striking contrast, the band structures for the CNT(5, 5)@BNNT(10, 10) under $F = 0$ and $F = 0.25$ V/Å are quite similar. The same phenomenon has been found for CNT (6, 6)@BNNT(10, 10) and CNT (7, 7)@BNNT(12, 12) DWHNTs when F is smaller than critical F_c (here F_c is a boundary when $F > F_c$, the band structure of armchair CNT@BNNT would change abruptly, when $F < F_c$, and the band structure of armchair CNT@BNNT would keep original shape). See the results in Table 1(c); both CNT and BNNT single-walled nanotubes experience large structural changes after geometric optimization with increasing F. When $F = 0.25$ V/Å, optimized CNT(5, 5) was distortion.

However, with increasing F, the DOS of the CNT@BNNT is not a simple superposition of the DOS for the individual CNT and pristine BNNT under F. The peak heights for several particular states on the DOS are moderately strengthened or weakened due to the tube-tube interaction. To explore the origin of this phenomenon, the PDOS for C, B, and N in pristine CNT(5, 5), BNNT(10, 10), and CNT(5, 5)@BNNT(10, 10) under electric fields $F = 0$ and 0.25 V/Å was plotted, respectively, as shown in Figure 5. The calculated PDOS indicates that the p-states of carbon atoms contribute mainly to the energy levels near the Femi level. The p-states of boron and nitrogen in pristine BNNT are very sensitive to the F. However, the change is not obvious in the heterostructure, which maybe caused by the effect of the tube-tube interaction.

We also examined the electronic properties of the zigzag CNT (7, 0)@BNNT(16, 0) and CNT(10, 0)@BNNT(18, 0) under an electronic field. We found that with increasing F the band gap of zigzag CNT (7, 0)@BNNT(16, 0) decreases gradually, and the phenomena are similar to the single-wall CNT (7, 0) under an electronic field. Though the band structure of zigzag CNT(10, 0)@BNNT(18, 0) also decreases gradually with increasing F, it is different from the single-wall CNT(10, 0), because of the increasing intertube interactions.

4. Conclusions

The electronic structures of the double-wall hetero-nanotubes near the Fermi level are dominated by the p-electrons of carbon atoms; the band structure of the armchair DWHNTs is difficult to modulate with changing intertube distance. However, either changing intertube distance or imposing electric field is the efficient way to modulated the band structure of zigzag DWHNTs. Our results suggest an interesting avenue of exploring novel heterostructure of CNT@BNNT for potentially important applications in CNT@BNNT-based nanodevices.

Conflict of Interests

The authors declare that there is no conflict of interests regarding the publication of this paper.

Acknowledgments

This project was supported by the Natural Science Foundation of China (Grant no. 51402251), the Natural Science Foundation of Jiangsu Province of China (Grant no. BK20140471), and Talent Introduction Project of Yancheng Institute of Technology (nos. XKR2011009 and XKR2011001).

References

[1] C. R. Dean, A. F. Young, I. Meric et al., "Boron nitride substrates for high-quality graphene electronics," *Nature Nanotechnology*, vol. 5, no. 10, pp. 722–726, 2010.

[2] D. Usachov, V. K. Adamchuk, D. Haberer et al., "Quasifree-standing single-layer hexagonal boron nitride as a substrate for graphene synthesis," *Physical Review B*, vol. 82, no. 7, Article ID 075415, 2010.

[3] G. Giovannetti, P. A. Khomyakov, G. Brocks, P. J. Kelly, and J. Van Den Brink, "Substrate induced band gap in graphene on hexagonal boron nitride: *Ab* initio density functional calculations," *Physical Review B*, vol. 76, no. 7, Article ID 073103, 2006.

[4] J. Sławińska, I. Zasada, and Z. Klusek, "Energy gap tuning in graphene on hexagonal boron nitride bilayer system," *Physical Review B*, vol. 81, no. 15, Article ID 155433, 2010.

[5] A. Ramasubramaniam, D. Naveh, and E. Towe, "Tunable band gaps in bilayer graphene-BN heterostructures," *Nano Letters*, vol. 11, no. 3, pp. 1070–1075, 2011.

[6] R. Nakanishi, R. Kitaura, J. H. Warner et al., "Thin single-wall BN-nanotubes formed inside carbon nanotubes," *Scientific Reports*, vol. 3, article 1385, 2013.

[7] A. Gomathi, M. Ramya Harika, and C. N. R. Rao, "Urea route to coat inorganic nanowires, carbon fibers and nanotubes by boron nitride," *Materials Science and Engineering A*, vol. 476, no. 1-2, pp. 29–33, 2008.

[8] M. Das, A. K. Basu, S. Ghatak, and A. G. Joshi, "Carbothermal synthesis of boron nitride coating on PAN carbon fiber," *Journal of the European Ceramic Society*, vol. 29, no. 10, pp. 2129–2134, 2009.

[9] L. Chen, H. Ye, Y. Gogotsi, and M. J. McNallan, "Carbothermal synthesis of boron nitride coatings on silicon carbide," *Journal of the American Ceramic Society*, vol. 86, no. 11, pp. 1830–1837, 2003.

[10] S. Li, Y. F. Wu, W. Liu, and Y. H. Zhao, "Control of band structure of van der Waals heterostructures: silicene on ultrathin silicon nanosheets," *Chemical Physics Letters*, vol. 609, pp. 161–166, 2014.

[11] P. Avouris, R. Martel, V. Derycke, and J. Appenzeller, "Carbon nanotube transistors and logic circuits," *Physica B: Condensed Matter*, vol. 323, no. 1–4, pp. 6–14, 2002.

[12] C. L. Phillips, C. S. Yah, S. E. Iyuke, K. Rumbold, and V. Pillay, "The cellular response of *Saccharomyces cerevisiae* to multi-walled carbon nanotubes (MWCNTs)," *Journal of Saudi Chemical Society*, vol. 19, no. 2, pp. 147–154, 2015.

[13] K. Chikkadi, M. Muoth, W. Liu, V. Maiwald, and C. Hierold, "Enhanced signal-to-noise ratio in pristine, suspended carbon nanotube gas sensors," *Sensors and Actuators, B: Chemical*, vol. 196, pp. 682–690, 2014.

[14] A. Freitas, S. Azevedo, and J. R. Kaschny, "Effects of a transverse electric field on the electronic properties of single- and multi-wall BN nanotubes," *Solid State Communications*, vol. 153, no. 1, pp. 40–45, 2013.

[15] C.-W. Chen, M.-H. Lee, and S. J. Clark, "Band gap modification of single-walled carbon nanotube and boron nitride nanotube under a transverse electric field," *Nanotechnology*, vol. 15, no. 12, pp. 1837–1843, 2004.

[16] P. Ordejón, E. Artacho, and J. M. Soler, "Self-consistent order-N density-functional calculations for very large systems," *Physical Review B*, vol. 53, no. 16, Article ID R10441, 1996.

[17] D. Sánchez-Portal, P. Ordejón, E. Artacho, and J. M. Soler, "Density-functional method for very large systems with LCAO basis sets," *International Journal of Quantum Chemistry*, vol. 65, no. 5, pp. 453–461, 1997.

[18] J. P. Perdew, K. Burke, and M. Ernzerhof, "Generalized gradient approximation made simple," *Physical Review Letters*, vol. 77, no. 18, pp. 3865–3868, 1996.

[19] H. J. Monkhorst and J. D. Pack, "Special points for Brillouin-zone integrations," *Physical Review B*, vol. 13, no. 12, pp. 5188–5192, 1976.

[20] B. Delley, "An all-electron numerical method for solving the local density functional for polyatomic molecules," *The Journal of Chemical Physics*, vol. 92, no. 1, pp. 508–517, 1990.

[21] B. Delley, "From molecules to solids with the DMol^3 approach," *Journal of Chemical Physics*, vol. 113, no. 18, pp. 7756–7764, 2000.

[22] J. P. Perdew and Y. Wang, "Accurate and simple analytic representation of the electron-gas correlation energy," *Physical Review B*, vol. 45, no. 23, pp. 13244–13249, 1992.

[23] S. Li, Y. Wu, Y. Tu et al., "Defects in silicene: vacancy clusters, extended line defects, and di-adatoms," *Scientific Reports*, vol. 5, article 7881, 2015.

[24] W. Liu, A. Tkatchenko, and M. Scheffler, "Modeling adsorption and reactions of organic molecules at metal surfaces," *Accounts of Chemical Research*, vol. 47, no. 11, pp. 3369–3377, 2014.

[25] W. Liu, S. N. Filimonov, J. Carrasco, and A. Tkatchenko, "Molecular switches from benzene derivatives adsorbed on metal surfaces," *Nature Communications*, vol. 4, article 2569, 2013.

[26] W. Liu, J. Carrasco, B. Santra, A. Michaelides, M. Scheffler, and A. Tkatchenko, "Benzene adsorbed on metals: concerted effect of covalency and van der Waals bonding," *Physical Review B*, vol. 86, no. 24, Article ID 245405, 2012.

[27] J. Yuan and K. M. Liew, "Structural stability of a coaxial carbon nanotube inside a boron-nitride nanotube," *Carbon*, vol. 49, no. 2, pp. 677–683, 2011.

[28] V. Zólyomi and J. Kürti, "First-principles calculations for the electronic band structures of small diameter single-wall carbon nanotubes," *Physical Review B*, vol. 70, no. 8, Article ID 85403, 2004.

[29] S. V. Tishchenko, "Electronic structure of zigzag carbon nanotubes," *Low Temperature Physics*, vol. 32, no. 10, pp. 953–956, 2006.